

Sensitive Photoresists for Rapid Multiphoton 3D Laser Micro- and Nanoprinting

Pascal Kiefer,* Vincent Hahn, Martina Nardi, Liang Yang, Eva Blasco, Christopher Barner-Kowollik, and Martin Wegener

Driven by recent advances in rapid multiphoton single-focus 3D laser nanoprinting, multifocus variants thereof, and projection-based multiphoton 3D laser nanoprinting, the necessary average total laser powers from femto-second laser oscillators or even from amplified femtosecond laser systems have exceeded the Watt level. Aiming at ever faster 3D printing, there exist two options: Using yet more powerful lasers or searching for more sensitive photoresists allowing for higher speeds at comparable or lower power levels. Here, altogether more than 70 different photoresists from the literature and a few new candidates are reviewed with regard to effective multiphoton sensitivity. A dimensionless sensitivity figure-of-merit allows to directly compare data taken under sometimes vastly different conditions.

1. Introduction

3D additive manufacturing a.k.a. 3D printing is steadily gaining importance as a versatile fabrication tool in academia and industry.^[1] The three key technological challenges currently being explored can be summarized as “finer, faster, more”, “implying achieving finer features or smaller voxel sizes connected with better spatial resolution,^[2] increasing the manufacturing speed in terms of the number of 3D printed voxels per second (making the technology “scalable”),^[3] and making accessible more dissimilar materials as well as complex 3D multimaterial architectures.^[4,5] In the ongoing quest for the advanced 3D printing technology, optics-based approaches play a prominent role, including one-photon-absorption based

(nonscanning) parallel projection technologies,^[6–8] computed axial lithography as an inverse tomography approach based on multiple 2D optical one-photon exposures from multiple different directions,^[9,10] and different forms of multiphoton-absorption 3D printing,^[11–16] mostly based on femto-second or picosecond pulsed lasers. Two-photon lithography has been pioneered by Maruo et al. in 1997.^[17] In a few exceptions, continuous-wave (cw) lasers have been used.^[18,19]

Going “faster” can mean scanning a single focus faster,^[20] adapting multiple foci approaches,^[21,22] scanning multiple foci faster,^[3] or printing more voxels/pixels in parallel per unit time in projection-based approaches without scanning in the focal plane,^[6,7,9,10,12] yet scanning normal to the focal plane. In any case, increasing the printing rate is inherently connected to either using more laser power and the same photoresist, or to using comparable or less laser power by exploiting optimized more sensitive photoresists. As femtosecond or picosecond laser power is a precious commodity associated with a considerable fraction of the cost of most advanced 3D multiphoton laser printers, we dedicate the main part of this contribution to a screening of sensitive multiphoton-absorption-based photoresists. These photoresists are either taken from the published literature, reproduced and remeasured in our labs, or are newly investigated herein as promising candidates.

P. Kiefer, V. Hahn, Dr. L. Yang, Dr. E. Blasco, Prof. C. Barner-Kowollik, Prof. M. Wegener
3DMM2O-Cluster of Excellence (EXC-2082/1-390761711)
Karlsruhe Institute of Technology (KIT) and Heidelberg University
Karlsruhe 76131, Germany
E-mail: Pascal.Kiefer@kit.edu

P. Kiefer, V. Hahn, Dr. L. Yang, Prof. M. Wegener
Institute of Applied Physics (APH)
Karlsruhe Institute of Technology (KIT)
Karlsruhe 76128, Germany

 The ORCID identification number(s) for the author(s) of this article can be found under <https://doi.org/10.1002/adom.202000895>.

© 2020 The Authors. Published by Wiley-VCH GmbH. This is an open access article under the terms of the Creative Commons Attribution License, which permits use, distribution and reproduction in any medium, provided the original work is properly cited.

DOI: 10.1002/adom.202000895

V. Hahn, Dr. M. Nardi, Dr. L. Yang, Dr. E. Blasco, Prof. C. Barner-Kowollik, Prof. M. Wegener
Institute of Nanotechnology (INT)
Karlsruhe Institute of Technology (KIT)
Karlsruhe 76128, Germany

Dr. M. Nardi, Dr. E. Blasco, Prof. C. Barner-Kowollik
Macromolecular Architectures
Institute of Chemical Technology and Polymer Chemistry (ITCP)
Karlsruhe Institute of Technology (KIT)
Karlsruhe 76128, Germany

Prof. C. Barner-Kowollik
School of Chemistry and Physics
Queensland University of Technology (QUT)
2 George Street, Brisbane, QLD 4000, Australia

Prof. C. Barner-Kowollik
Centre for Materials Science
Queensland University of Technology (QUT)
2 George Street, Brisbane, QLD 4000, Australia

At first sight, a sensitive multiphoton photoresist merely requires a certain density of strongly absorbing photoinitiator molecules within the photoresist. Indeed, substantial efforts have been dedicated to designing, synthesizing, and characterizing photoinitiator molecules exhibiting large two-photon-absorption cross sections at certain wavelengths.^[23–35] However, it has become evident from recent detailed one-photon-absorption experiments^[36] that the absorption spectrum versus wavelength may peak at a completely different wavelength than the spectrum of the corresponding light-induced polymerization rate.^[36,37] Importantly, this surprising and not-well-understood finding refers to optically thin samples. In optically thick samples, such behavior may occur as an artifact. Transferring this finding to multiphoton absorption implies that it is generally not sufficient to search for photoinitiators exhibiting large two-photon-absorption cross sections, but one must rather search for the sensitivity of the entire process starting with the absorption of light by a molecule and ending with a cross-linked network (at least for negative-tone photoresists). In other words, photoresist design and optimization is truly a materials-science issue. Unfortunately, on a microscopic level, the underlying processes are currently not well understood.^[36]

In a few exceptional cases, using laser exposure wavelengths at around $\lambda_0 = 400$ nm, multiphoton photoresists without extra photoinitiator molecules have been reported. This includes experiments using a quasi-cw laser^[38] and using femtosecond lasers.^[39,40] In these experiments, we assume that the incident laser directly excites the HOMO–LUMO (highest occupied molecular orbital–lowest unoccupied molecular orbital) transition of the underlying monomer by multiphoton absorption. The processes following this initial absorption are not fully clear.

A wealth of experimental observations on sensitive photoresists has been published in the literature. Yet, these studies not only refer to different types of photoinitiators (if any), but also to different photoinitiator concentrations n_{PI} , different monomers used, different additives, such as quenchers or coinitiators, different free-space laser wavelengths λ_0 , different numerical apertures of the focusing microscope lenses NA, different focus velocities v , different necessary average threshold laser powers P_{th} , different laser pulse durations t_p , possibly different levels of pulse chirping, and different laser pulse repetition rates R_p . This situation hampers the direct comparison of photoresists with respect to their sensitivity under relevant conditions.

Therefore, herein, we proceed as follows. We briefly recapitulate the point of using two-photon absorption rather than one-photon absorption in Section 2. We compare single-focus scanning and multiple-focus scanning in terms of the necessary average optical laser powers in Section 3. We motivate and define in Section 4 a simple photoresist-sensitivity figure-of-merit (FOM) that reduces the complexity concerning photoresist sensitivity into a single dimensionless number for any given experiment on a given photoresist system. In Section 5, we collect a large number of data from the published literature, add a few further candidates, and map all of them (a total of more than 70) onto the defined sensitivity FOM. Our experiments on the new candidates are described in Section 6. We finally conclude in Section 7.

2. Why Two-Photon Absorption?

For most relevant (negative-tone) photoresists, the incident light induces a chemical reaction via a photoinitiator molecule. This reaction cures a liquid monomer to a solidified cross-linked polymer. In the following development step, a solvent such as, for example, acetone washes out insufficiently cross-linked molecules, leaving behind the final 3D printed structure. Despite the complex and not fully understood reaction-diffusion kinetics of the photoresist (see, e.g.,^[41–43]), two simple assumptions, A) and B) respectively, concerning the photoresist are usually a good starting point to describe the behavior.

- A) The threshold model: Below a certain local exposure dose—the (gelation) threshold dose—the material is not sufficiently crosslinked. Hence, it is washed out in the development step. In regions where the exposure dose is above this threshold dose, the material is sufficiently cross-linked and remains after the development. Thereby, the threshold model basically “digitizes” the exposure dose to “material” or “no material”. Within the threshold model, arbitrarily small features or voxels can be printed.^[2,11,42] There is no limit imposed by diffraction of light.^[2]
- B) The accumulation model: If the photoresist is subject to two or more point exposures at the same location or at different locations, the photoresist integrates the corresponding exposure doses. On this basis, as explained in detail in ref. [2], one obtains a minimum separation between adjacent separated features. Precisely, the two-photon Sparrow criterion determines the diffraction-limited resolution.^[2] Moreover, within the accumulation model, it is not possible to 3D print arbitrary complex 3D architectures using one-photon absorption, whereas this is possible using two-photon absorption or multiphoton absorption.

The latter statement is *the* critical motivation for using two-photon absorption for 3D printing and is hence illustrated in **Figure 1**. For one-photon absorption shown in the first row of Figure 1, the exposure dose D_{exp} is proportional to the light intensity, $D_{exp} \propto I$. For two-photon absorption shown in the second row of Figure 1, the exposure dose is proportional to the squared intensity, $D_{exp} \propto I^2$. To counteract the possible misunderstanding that the main benefit of two-photon absorption is a smaller voxel size than for one-photon absorption, we choose $\lambda_0 = 800$ nm free-space wavelength for two-photon absorption and $\lambda_0/2 = 400$ nm free-space wavelength for one-photon absorption. As a result, the individual voxels shown in column (a) of Figure 1 for one-photon absorption (1PA) are significantly smaller than those for two-photon absorption (2PA). For both cases, we consider a laser focus with a numerical aperture of NA = 1.4. In the calculation of the electromagnetic fields in the laser focus, we use the Debye approximation as in ref. [44]. For both, one-photon absorption and two-photon absorption, by virtue of the threshold model, arbitrarily small voxels can be printed in 3D. We emphasize that, so far, there is no point of using two-photon absorption instead of one-photon absorption. In panels (b–d), we raster scan the laser focus over a small square and four legs, mimicking a simple table. We assume that the total exposure dose is given by the sum of the

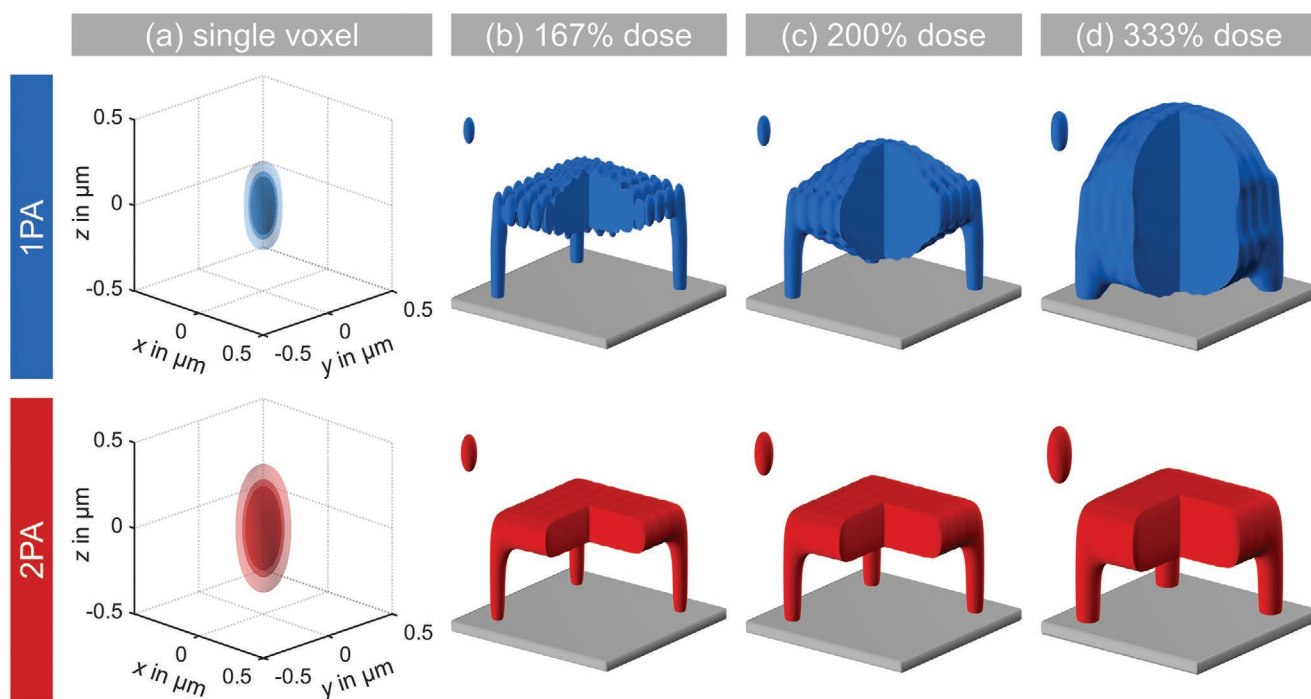


Figure 1. Illustration of 3D laser nanoprinting with a numerical aperture of $NA = 1.4$. In the first row, we consider one-photon absorption (1PA) at wavelength $\lambda_0/2 = 400$ nm with an exposure dose proportional to the intensity of light, $D_{\text{exp}} \propto I$. In the second row, we consider two-photon absorption (2PA) at fundamental wavelength $\lambda_0 = 800$ nm with an exposure dose proportional to the squared intensity, $D_{\text{exp}} \propto I^2$. In column (a), we assume the photoresist threshold model and show resulting structures for single-voxel exposure doses of 167%, 200%, and 333%, displayed by three isosurfaces. At a single-voxel exposure dose defined by 100%, the peak of the dose profile of a single voxel is at the threshold and, hence, only a singular point results. In columns (b–d), we additionally assume the photoresist accumulation model and sum up sequential exposure doses as shown in column (a), aiming at 3D printing a table, composed of a plate and four legs. The in-plane voxel spacing used for the plate is $0.2 \mu\text{m}$. The used single-voxel exposure doses are indicated at the top. Note the huge proximity effect for 1PA despite the smaller voxel size for 1PA.

individual exposure doses. At the end, we apply the threshold model to the accumulated exposure dose. For one-photon absorption, the table plate is thicker in the middle. This thickening rapidly increases with increasing exposure dose, leading to a prominent largely overexposed region for 333% dose in the upper row of Figure 1d. A thickening of the plate versus increasing dose is found for two-photon absorption in the lower row of Figure 1 as well, but the thickness of the plate remains roughly constant throughout the plate.

The described distortions can be readily understood intuitively: At some point in the tail of the focus, which has a Lorentzian shape on the optical axis in the axial direction,^[45] the intensity may be only 1% of its peak in the center of the focus. Upon scanning, and within the accumulation model, these tail exposures add up, for example 100 times, in which case the residual exposure dose is $100 \times 1\% = 100\%$. This explains the distortions in the first row of Figure 1. The two-photon absorption rate is $\propto I^2$. This means that the 1% tail exposure for one-photon absorption turns into a $(1\%)^2 = 10^{-4}$ tail exposure for two-photon absorption. Even after adding up this tail exposure 100 times due to scanning the focus, the parasitic exposure dose is merely $100 \times 10^{-4} = 1\%$. The problem with the tails is not fully solved, but has become much less pronounced by using two-photon absorption. Importantly, any process that leads to an exposure rate $D_{\text{exp}} \propto I^2$ rather than $D_{\text{exp}} \propto I$ (one-photon absorption) will suppress the tails. Multiphoton absorption

$D_{\text{exp}} \propto I^m$ with integer $m > 2$ is obviously even better to reduce the effect of the tails. Finally, we emphasize once again that the discussion in this section so far has been based on the accumulation model (B).

A few publications successfully using cw lasers^[18,19] for the making of 3D microstructures suggest that the accumulation model (B) has its limits under certain conditions. For example, the Schwarzschild effect based on the complex local reaction diffusion kinetics^[41,43] introduces an effective nonlinearity even for strict one-photon absorption.

C) The “forgetting photoresist” model. The polar opposite of the photoresist accumulation model (B) is described by a photoresist that completely “forgets” all below-threshold exposures, for example by fast enough diffusion of small oligomers to regions sufficiently far away from the excitation focus. Such a “forgetting photoresist”^[2] would completely change the picture because the above tail-accumulation argument becomes obsolete (cf. Figure 1). There simply would not be any tails. In other words, one could 3D print arbitrary complex 3D architectures by using one-photon absorption and a low-power continuous-wave laser. Furthermore, such a “forgetting photoresist” would not underlie any restrictions in terms of spatial resolution due to optical diffraction.^[2] Neither the Abbe diffraction barrier nor the two-photon Sparrow criterion^[2] would apply.

3. Single-Focus 3D Printing versus Multiple Foci

As this paper is concerned with minimizing the laser power necessary for multiphoton 3D laser printing, it is interesting to briefly recapitulate whether—for a given fixed photoresist—3D printing using a single laser focus or using an integer number of $N \geq 1$ foci leads to a lower required total average laser power P .

Let us consider only two-photon absorption with $m = 2$ (all of our findings can easily be generalized to m -photon absorption with integer $m \neq 2$). The individual focus velocity shall be v . We aim at a constant target printing rate, p , in units of voxels s^{-1} . The voxel size or diameter shall be d , leading to $p = Nv/d$, hence

$$v = pd/N \quad (1)$$

Furthermore, the two-photon transition rate is proportional to $P_1^m = P_1^2$, with the power P_1 for one laser focus. For fixed constant exposure dose of one voxel, the product of exposure time and P_1^2 needs to be constant. The exposure time is $\propto 1/v$, leading to $P_1^2/v = \text{const}$. With the total power for N foci $P = NP_1$ (assuming negligibly small interference effects among the foci), we obtain

$$P \propto N\sqrt{v} \quad (2)$$

Figure 2 visualizes these two simple Equations (1) and (2) for v and P in a $P(v)$ diagram in double-logarithmic representation. The vertical power scale is in arbitrary units because the absolute powers depend on the sensitivity of the photoresist used.

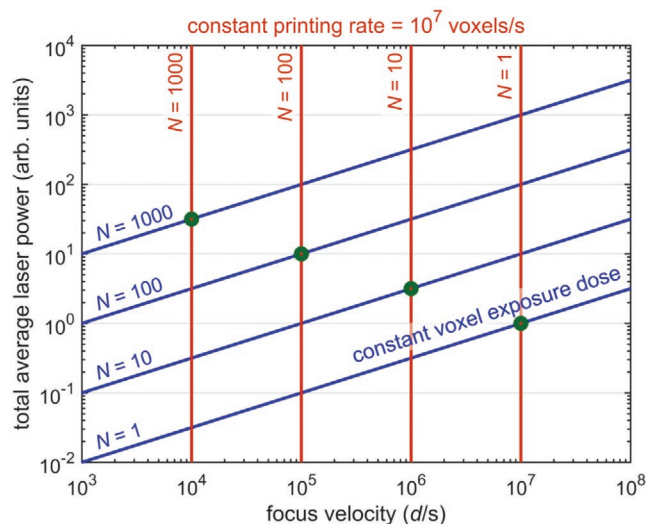


Figure 2. Illustration for two-photon 3D laser printing with an integer number N of foci scanned in parallel. For clarity, only $N = 1$, $N = 10$, $N = 100$, and $N = 1000$ are shown. Lines of constant voxel exposure dose (blue) and lines of constant printing rate (red) in units of voxels/s are plotted versus the focus velocity on the horizontal axis (logarithmic scale) and versus the total average laser power on the vertical axis (logarithmic scale). The intersections of the blue and red curves are the possible solutions, which are highlighted by the green circles. Clearly, the solution for a single focus ($N = 1$) leads to the lowest total laser power, but also to the largest necessary focus velocity. The vertical scale has arbitrary units because the absolute power levels depend on the sensitivity of the multiphoton photoresist used.

Figure 2 refers to a given and fixed photoresist sensitivity. The solutions of the problem are the crossing points, which we have highlighted by the green circles. Clearly, the problem has different solutions for different integers N . These solutions correspond to different necessary total laser powers P . Obviously, the solution with the lowest power corresponds to $N = 1$ (in contrast, for one-photon absorption, all solutions correspond to the same power P , not depicted). This means that it is best to 3D print using a single laser focus rather than using multiple foci—provided that the necessary focus velocity v is achievable experimentally. Generally, the choice of the solution, i.e., the choice of N , depends on whether the experiment is limited by the available average laser power or limited by the accessible maximum focus velocity. Using multiple foci makes sense if the focus velocity is a limiting factor. This situation has applied for our recent work,^[3] where we used $N = 3 \times 3 = 9$ foci, leading to a total peak printing rate of nearly 10^7 voxels s^{-1} .

In the light of the above discussion, projection-based multiphoton 3D laser printing^[12] can be seen as a case of extremely large N , where the focus scanning velocity v is replaced by the axial velocity, i.e., by the layer thickness (or effective voxel height) divided by the exposure time for one plane.

4. A photoresist Sensitivity Figure-of-Merit (FOM)

Let us consider $N = 1$ from here on. Typical pulse peak intensities, I , required for two-photon-absorption induced polymerization of negative-tone photoresists for 3D laser nanoprining are in the range of about $I = 1 \text{ TW cm}^{-2} = 10^{12} \text{ W cm}^{-2} = 10^{16} \text{ W m}^{-2}$,^[46] give and take an order of magnitude. The pulse peak intensity of a periodically pulsed focused laser can be estimated from its average laser power P (in units of W), the pulse duration t_p (in units of s), the pulse repetition rate R_p (in units of s^{-1}), and the effective laser spot radius r (in units of m) via

$$I = \frac{P}{R_p t_p} \frac{1}{\pi r^2} \quad (3)$$

For the special case of a continuous-wave (cw) laser, we have $R_p t_p = 1$. The radius r of an ideal Gaussian focus, precisely, the point at which the intensity reaches $1/e^2$ of the spatial peak, is given by^[45]

$$r = \frac{\lambda_0}{\pi \text{NA}} \quad (4)$$

The factor π in the denominator can be discussed, but drops out below anyway. Furthermore, we inappropriately made use of the small-angle approximation. However, the thereby resulting error is comparably small to other uncertainties in our analysis. Hence, the spatial and temporal peak intensity is given by

$$I = \frac{P}{R_p t_p} \frac{(\pi \text{NA})^2}{\pi \lambda_0^2} \quad (5)$$

The following experimental imperfections (1–4) can reduce the peak pulse intensity with respect to this value. Therefore, the expression for I represents an upper bound. 1) The

laser pulses can be chirped due to the group-delay dispersion accumulated in optical materials or components in the beam path, which means that the pulse peak power and the peak intensity I decrease for a given average power P and that the pulse length increases. Most optical setups in the literature and all presently commercially available machines do not report on compensating for the group-delay dispersion, the effects of which tend to become more severe when going from the red to the blue end of the visible spectrum. The effect can be drastic. For example, in our recent work at around $\lambda_0 = 790$ nm,^[3] the measured pulse duration t_p increased by about a factor of ten from the output of the laser (about 100 fs) to the focal spot (about 1 ps). We compensated this temporal stretching by a prism-based arrangement.^[3] 2) Not all of the laser power may actually pass through the aperture at the entrance pupil of the focusing microscope lens (case of “over-illuminated” entrance pupil). 3) The power may refer to a position in front of the microscope lens rather than to the focal position. Typical relevant microscope lenses have an optical transmittance on the order of $T = 70\%$. Aspects (2) and (3) are not relevant if the power has been measured and quoted behind the microscope lens. Otherwise, we will generically assume full illumination of the aperture and $T = 70\%$ (unless a specific value has been quoted in the reference under discussion). 4) The aperture of the microscope lens may have been under-illuminated or the laser-beam wavefront is aberrated, in which case the effective numerical aperture is lower than the numerical aperture of the microscope lens, thus the power required to achieve a certain peak intensity is larger than it would have been ideally. All of these possible experimental shortcomings (1–4) make the peak laser intensity in the focus lower than it could have been and therefore reduce the sensitivity FOM (to be defined below) based on the reported experimental numbers to a value lower than it could have been if these errors had not been made.

Next, the multiphoton exposure dose, D_{exp} , deposited during an exposure time t_{exp} (typically with $t_{\text{exp}} \gg t_p$) by the mode-locked train of femto- or picosecond laser pulses is given by

$$D_{\text{exp}} = s_2 t_{\text{exp}} (R_p t_p) I^2 \quad (6)$$

The coefficient s_2 describes the effective two-photon sensitivity of the photoresist. The exposure time can be estimated by

$$t_{\text{exp}} = \frac{2r}{\nu} \quad (7)$$

where ν is again the focus velocity in units of m s^{-1} (the prefactor of 2 could be discussed, but drops out below anyway). In summary, the exposure dose D_{exp} , which needs to be kept constant to achieve a certain sufficiently large cross-linking density of the photoresist, is given by

$$D_{\text{exp}} = s_2 \frac{2\lambda_0}{\nu \pi \text{NA}} (R_p t_p) \left(\frac{P}{R_p t_p} \frac{(\pi \text{NA})^2}{\pi \lambda_0^2} \right)^2 \quad (8)$$

Solving for s_2 leads to

$$s_2 = \text{const.} \nu P_{\text{th}}^{-2} \lambda_0^3 R_p t_p (\text{NA})^{-3} \quad (9)$$

with $\text{const.} = D_{\text{exp}} / (2\pi)$. Here, P_{th} refers to the minimum average laser power, the threshold power, which still leads to a sufficiently cross-linked material after the exposure process under these conditions. To eliminate the unknown prefactor and to arrive at reasonable dimensionless values for the FOM, we define

$$\text{FOM} = \frac{s_2}{\tilde{s}_2} \quad (10)$$

where \tilde{s}_2 is a hypothetical reference two-photon photoresist with the following properties: $\tilde{\nu} = 1 \text{ m s}^{-1}$, $\tilde{P}_{\text{th}} = 1 \text{ W}$, $\tilde{\lambda}_0 = 1 \mu\text{m}$, $\tilde{R}_p = 100 \text{ MHz}$, $\tilde{t}_p = 100 \text{ fs}$, and $\tilde{\text{NA}} = 1$. In other words, the FOM is given by the formula

$$\text{FOM} = \nu P_{\text{th}}^{-2} \lambda_0^3 R_p t_p (\text{NA})^{-3} \quad (11)$$

if ν is inserted in units of m s^{-1} , P_{th} in units of W , λ_0 in units of μm , R_p in units of 100 MHz , and t_p in units of 100 fs . NA is dimensionless.

A single sensitivity FOM value alone has no meaning. The FOM becomes meaningful when comparing the sensitivity FOM values of two or more different photoresists. The larger the FOM, the more sensitive the photoresist system.

The following examples (1)–(5) shall illustrate the FOM according to (11). 1) Consider two publications using the exact same two-photon photoresist, the same wavelength, the same repetition rate, the same scan speed, the same NA, but two different pulse lengths t_p . As a result, the two publications would have measured two different threshold laser powers P_{th} . Insertion into (11) would lead to the same FOM. 2) Consider two publications using the exact same two-photon photoresist, the same wavelength, the same repetition rate, the same NA, the same pulse length t_p , but two different scan velocities ν . As a result, the two publications would have measured two different threshold laser powers P_{th} . Insertion into (11) would again lead to the same FOM. 3) A four times larger FOM leads to a two times lower threshold power P_{th} at otherwise fixed parameters. 4) Reducing the free-space wavelength λ_0 by a factor of 2 (e.g., from 800 to 400 nm), for otherwise constant parameters, decreases the FOM by a factor of $2^3 = 8$. 5) The FOM indirectly depends on the photoinitiator concentration n_{PI} : If a publication on a certain photoresist system has used a lower concentration n_{PI} than what would have been possible given the solubility limit, the threshold power P_{th} has been higher, and thus the FOM is lower than what would have been possible.

A subset of the publications that we refer to in Section 4 indeed uses a constant focus scanning velocity ν . However, another subset of references instead uses a fixed focus position (i.e., $\nu = 0$) and quotes the exposure time t_{exp} and power P_{th} at the threshold. In order to include these publications into our screening of photoresists with respect to sensitivity as well, using Equations (4) and (7) from above, we convert their data into an effective velocity

$$\nu_{\text{eff}} = \frac{2\lambda_0}{\pi \text{NA} t_{\text{exp}}} \quad (12)$$

and insert ν_{eff} according to (12) instead of ν into formula (11) for the sensitivity FOM.

To summarize this section, the spirit of the defined dimensionless two-photon-absorption based photoresist-sensitivity

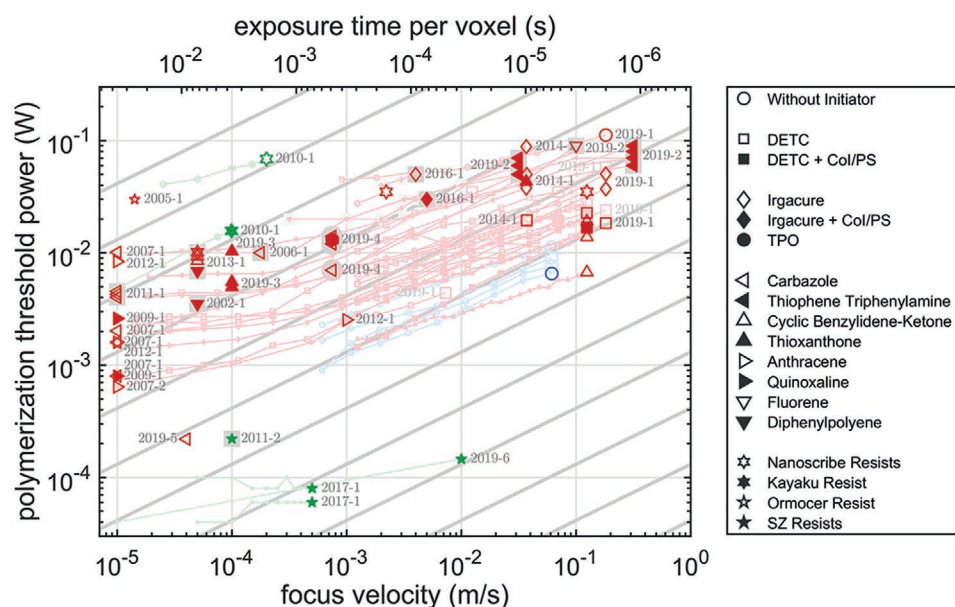


Figure 3. The threshold laser power P_{th} (logarithmic scale) for various multiphoton photoresist systems is plotted versus the focus scanning velocity ν (logarithmic scale). The upper horizontal scale provides the effective exposure time t_{exp} (for a voxel size of 364 nm, corresponding to $\lambda_0 = 800$ nm exposure wavelength) that is equivalent to ν . The color of the symbols roughly indicates the exposure wavelength. The various symbol types are explained in the legend. For simplicity, only the photoinitiator classes have been indicated except for last group (star symbols) where the names of the commercially available photoresist are given. For the data points indicated by the gray background, no threshold power is available and we have instead taken a typical 3D printing power. Hence, these points have to be taken with some caution. Data points with bright colors indicate measurements of the same photoinitiator but different monomer. Small data points connected by lines indicate measurements of the same photoresist but varying focus velocity. Measurements without labels have been performed by us. The raw data underlying all data points are provided in Tables 1 and 2. Furthermore, a few data points on SZ photoresists, which exhibit unusual low polymerization threshold powers at low laser repetition rates, are not included in this graph for the sake of clarity. They are shown in Figure 4 and specified in Tables 1 and 2. The parallel gray straight lines with a slope of 1/2 correspond to the scaling $P_{th} \propto \sqrt{\nu}$.

FOM is that it assesses what has actually been accomplished and not what could have been accomplished by either modifying the photoresist system or by eliminating shortcomings of the measurement setup or combinations thereof. The sensitivity FOM aims at being a photoresist material property, and does ideally not depend on the properties of the measurement setup or the measurement conditions. In particular, it ideally does not depend on the focus velocity ν .

5. Review of Photoresist Systems

In **Figure 3**, we plot the threshold laser power P_{th} versus the focus velocity ν (at which these data have been taken) on a double-logarithmic scale. The references and the raw input data of all data points shown in **Figure 3** are given in **Tables 1** and **2**. No corrections of any sort have been performed. The upper horizontal scale shows the exposure time t_{exp} corresponding to ν . This additional scale is necessary because some data have been taken for fixed focus position, i.e., for $\nu = 0$ (see Section 4), and finite exposure time t_{exp} at this fixed position. The set of logarithmic straight lines with a slope of 1/2 illustrates the scaling $P_{th} \propto \sqrt{\nu}$ expected for ideal two-photon absorption.

For some of the data points (see **Tables 1** and **2**), no threshold powers are available from the published literature. To include these data as well, we have taken the power quoted in these publications required to 3D print a structure.

Due to the accumulation of exposure dose (“proximity effect”) when printing entire structures rather than point exposures or simple isolated lines, these powers can be lower than the threshold power. They may also be higher than the threshold power. We cannot know. Thus, these data points have to be taken with caution. We have indicated them in **Figure 3** by a gray background.

As discussed in Section 4, all the data shown in **Figure 3** are difficult to compare directly because they have been taken under vastly different conditions. Therefore, in **Figure 4**, we show the same data as in **Figure 3**, but converted into the dimensionless sensitivity FOM described in Section 4. Here, in principle, the horizontal focus-velocity axis is not necessary as the FOM should ideally not depend on the focus velocity ν . However, we keep this axis to ease the comparison with **Figure 3** and to indicate at which velocities these data have actually been taken. A much more interesting quantity to be plotted on the horizontal axis would have been the minimum consistently attainable feature size for a given material. For instance, one straight-forward way of sensitizing a photoresist is to deplete it from solvated oxygen.^[41] However, this leads to pronounced proximity effects and a loss of resolution.^[41] Unfortunately, the data availability for minimum feature sizes or voxel sizes is scarce, especially when combined with photoresist sensitivity data.

The symbols in **Figures 3** and **4** indicate different photoresists, the colors of the symbols encode the used exposure wavelength. Dark red symbols correspond to about $\lambda_0 = 1000$ nm wavelength,

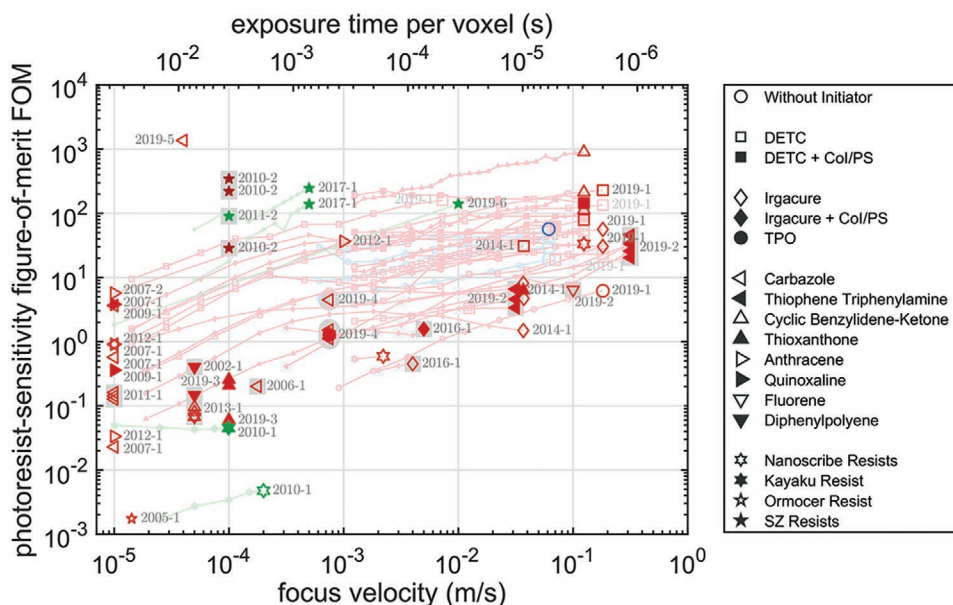


Figure 4. As Figure 3, but the reported laser power of all data points is converted into the dimensionless photoresist-sensitivity figure-of-merit (FOM). Ideally, for a given two-photon photoresist, the FOM should *not* depend on the focus scanning velocity ν .

red to about $\lambda_0 = 800$ nm wavelength, green to about $\lambda_0 = 532$ nm wavelength, and blue to about $\lambda_0 = 400$ nm wavelength. The precise wavelengths are given in Tables 1 and 2.

In Figure 4, the sensitivity FOM of the various photoresists varies by about six orders of magnitude. Due to the large number of entries, it is not meaningful to discuss the individual data points. We emphasize once again that, for a given two-photon-absorption-based photoresist, the FOM—by its definition—does *not* depend on ν .

Sadly, we do not see any clear trends or correlations of the photoresist sensitivity with respect to the chemistry of the photoresist composition in Figure 4. Therefore, for what follows in this section, we only discuss three groups of data points with sensitivity FOM exceeding 100.

Among the most sensitive photoresist systems that have successfully been tested and applied at large focus velocities is PETA (pentaerythritol triacrylate) as monomer and DETC (7-diethylamino-3-thenoylcoumarin) as a commercially available photoinitiator.^[47] This system is exceptional in different regards. First, the concentration of the photoinitiator is lower by an order of magnitude than what is commonly used for other photoinitiators. Naively, low concentration leads to low sensitivity (see Section 4). Unfortunately, the concentration of DETC in PETA cannot be increased due to its solubility limit. Second, under these conditions, DETC shows two-photon induced fluorescence, indicating that the primary absorption is indeed a second-order process. However, the overall nonlinear behavior of DETC in PETA as a photoresist is not consistent with ideal two-photon absorption but is rather effectively a third-order process. This observation has been made previously when varying the laser pulse repetition rate^[48] and, independently, when varying the exposure time.^[43]

The mechanisms underlying this third-order behavior are not fully understood. Such behavior could generally result if, for example, two-photon absorption brings an electron from the

ground-state manifold to the excited-state manifold of the photoinitiator molecule, from where the electron relaxes into some lower-energy intermediate state with rather long lifetime. From there, one-photon absorption brings the electron to a state from which radicals can be generated. Overall, three photons need to be absorbed to start the chemical reaction. However, this simple picture fails to describe the complex behavior of DETC in regard to a possible depletion laser beam^[47,49] (which is not used here). As a result of its effective third-order behavior, the sensitivity FOM of DETC in PETA depends on the focus velocity ν . This behavior does not agree with the discussion in Section 4. Nevertheless, the threshold powers of DETC at large focus velocities are lower than those of many other photoresists (see Figure 3). Clearly, due to the third-order behavior, the effective sensitivity advantage of DETC increases with increasing focus velocity ν according to $FOM \propto \nu^{3/2}$, currently making it an attractive option for rapid 3D laser printing at around $\lambda_0 = 800$ nm laser wavelength.

A promising photoresist system composed of a photoinitiator containing donor and acceptor groups in a conjugated backbone is BDMeABnCHx ((2E,6E)-2,6-bis(4-(dimethylamino)benzylidene)-4-methylcyclohexanone) and the monomer BPADA (ethoxylated bisphenol A diacrylate). BDMeABnCHx reportedly has a high two-photon absorption cross-section, while being obtainable with a one-step synthesis.^[31] Our experiments show that the effective nonlinear behavior of BDMeABnCHx in BPADA, similar to that of DETC in PETA, is not a second-order process (see Figure 3). Furthermore, the sensitivity of the two photoresists is comparable, even though the concentration of BDMeABnCHx in BPADA is even lower than that of DETC in PETA due to solubility limitations. We discuss a modified and improved version of BDMeABnCHx in Section 6.

At yet higher focus velocities, or equivalently, at yet smaller exposure times, while keeping the exposure dose constant by increasing the peak laser power, four-photon absorption and

Table 1. The nomenclature in the second column connects the symbols shown in Figures 3 and 4 as well as in the first column with the reference numbers of this review listed in the third column. The fourth column provides the photoresist composition in a nomenclature extended with respect to the legends of Figures 3 and 4. More complete information on the photoresist composition and on other aspects is given in the file provided in the Supporting Information. The fifth column of this table lists the dimensionless photoresist-sensitivity figure-of-merit FOM (cf. vertical axis of Figure 4), the sixth column the corresponding scanning velocity ν (cf. horizontal axis of Figures 3 and 4). The threshold laser power P_{th} plotted on the vertical axis of Figure 3 is given in the seventh column. The following four columns provide the parameters which are necessary to convert the P_{th} values into the FOM values, namely the laser wavelength λ_0 , the laser pulse duration t_p , the pulse repetition rate R_p , and the microscope objective numerical aperture NA. The last column lists the used photoinitiator concentration n_{PI} .

Sym.	Label	Ref.	Photoresist	FOM	ν [m s ⁻¹]	P_{th} [W]	λ_0 [m]	t_p [s]	R_p [Hz]	NA	n_{PI} [wt%]
▼	2002-1	[25]	BSB-S ₂ + SU-8 + GBL	4.03×10^{-1}	5.00×10^{-5}	3.50×10^{-3}	7.45×10^{-7}	8.0×10^{-14}	8.2×10^7	1.40	2.500
★	2005-1	[13]	Irg369 + ORMOCER I	1.74×10^{-3}	1.42×10^{-5}	3.00×10^{-2}	7.80×10^{-7}	8.0×10^{-14}	8.0×10^7	1.40	0.250
◁	2006-1	[26]	BMPyPCbzTos + MA + DEP-6A	2.01×10^{-1}	1.77×10^{-4}	1.00×10^{-2}	7.80×10^{-7}	8.0×10^{-14}	8.2×10^7	1.40	0.100
◁	2007-1	[27]	BCPhPnCbz + MAA + DEP-6A	2.29×10^{-2}	1.00×10^{-5}	1.01×10^{-2}	8.00×10^{-7}	8.0×10^{-14}	8.0×10^7	1.42	0.720
◁	2007-1	[27]	BCPhPnCbz + MAA + DEP-6A	9.12×10^{-1}	1.00×10^{-5}	1.60×10^{-3}	8.00×10^{-7}	8.0×10^{-14}	8.0×10^7	1.42	0.750
◁	2007-1	[27]	BNPhPnCbz + MAA + DEP-6A	5.72×10^{-1}	1.00×10^{-5}	2.02×10^{-3}	8.00×10^{-7}	8.0×10^{-14}	8.0×10^7	1.42	0.770
◁	2007-1	[27]	BNPhPnCbz + MAA + DEP-6A	3.65×10^0	1.00×10^{-5}	8.00×10^{-4}	8.00×10^{-7}	8.0×10^{-14}	8.0×10^7	1.42	0.800
▷	2007-2	[28]	BPnDPHant + MAA + DPHA	5.70×10^0	1.00×10^{-5}	6.40×10^{-4}	8.00×10^{-7}	8.0×10^{-14}	8.0×10^7	1.42	0.367
▶	2009-1	[29]	BTPHAQ + MAA + DPHA	3.81×10^0	1.00×10^{-5}	8.00×10^{-4}	8.00×10^{-7}	8.0×10^{-14}	8.0×10^7	1.40	0.500
▶	2009-1	[29]	BTPHABnQ + MAA + DPHA	3.61×10^{-1}	1.00×10^{-5}	2.60×10^{-3}	8.00×10^{-7}	8.0×10^{-14}	8.0×10^7	1.40	0.500
★	2010-1	[18]	SU-8	4.52×10^{-2}	9.92×10^{-5}	1.57×10^{-2}	5.32×10^{-7}	cw	cw	1.40	?
★	2010-1	[18]	IP-L	4.75×10^{-3}	2.00×10^{-4}	6.87×10^{-2}	5.32×10^{-7}	cw	cw	1.40	?
★	2010-2	[16]	Irg369 + SZ2080	2.21×10^2	1.00×10^{-4}	2.33×10^{-6}	1.03×10^{-6}	3.0×10^{-13}	1.0×10^3	1.40	1.000
★	2010-2	[16]	DABP + SZ2080	3.45×10^2	1.00×10^{-4}	1.86×10^{-6}	1.03×10^{-6}	3.0×10^{-13}	1.0×10^3	1.40	1.000
★	2010-2	[16]	Pure SZ2080	2.86×10^1	1.00×10^{-4}	6.46×10^{-6}	1.03×10^{-6}	3.0×10^{-13}	1.0×10^3	1.40	0.000
◁	2011-1	[35]	BNPhBnC + MAA	1.61×10^{-1}	1.00×10^{-5}	4.02×10^{-3}	7.80×10^{-7}	1.0×10^{-13}	8.2×10^7	1.45	0.100
◁	2011-1	[35]	BNPhBnC/PhOMe + MAA	1.42×10^{-1}	1.00×10^{-5}	4.28×10^{-3}	7.80×10^{-7}	1.0×10^{-13}	8.2×10^7	1.45	0.100
◁	2011-1	[35]	BNPhMBnC + MAA	1.27×10^{-1}	1.00×10^{-5}	4.53×10^{-3}	7.80×10^{-7}	1.0×10^{-13}	8.2×10^7	1.45	0.100
★	2011-2	[14]	DETX + SZ2080	9.02×10^1	1.00×10^{-4}	2.21×10^{-4}	5.32×10^{-7}	8.0×10^{-12}	1.0×10^6	1.40	1.000
▷	2012-1	[30]	BDAPhPnOAnt + MAA + DPHA	3.65×10^1	1.00×10^{-3}	2.53×10^{-3}	8.00×10^{-7}	8.0×10^{-14}	8.0×10^7	1.42	0.940
▷	2012-1	[30]	BPTPnOAnt + MAA + DPHA	9.12×10^{-1}	1.00×10^{-5}	1.60×10^{-3}	8.00×10^{-7}	8.0×10^{-14}	8.0×10^7	1.42	0.867
▷	2012-1	[30]	BCPhPnOAnt + MAA + DPHA	3.33×10^{-2}	1.00×10^{-5}	8.37×10^{-3}	8.00×10^{-7}	8.0×10^{-14}	8.0×10^7	1.42	0.899
▼	2013-1	[31]	DBAn2PhOMe + TTA + ETA	1.47×10^{-1}	5.00×10^{-5}	6.87×10^{-3}	7.80×10^{-7}	1.0×10^{-13}	8.0×10^7	1.40	0.377
▽	2013-1	[31]	BDBAn3FL + TTA + ETA	6.76×10^{-2}	5.00×10^{-5}	1.01×10^{-2}	7.80×10^{-7}	1.0×10^{-13}	8.0×10^7	1.40	0.400
△	2013-1	[31]	BDMAnPhPn + TTA + ETA	9.59×10^{-2}	5.00×10^{-5}	8.49×10^{-3}	7.80×10^{-7}	1.0×10^{-13}	8.0×10^7	1.40	0.202
△	2013-1	[31]	BDBuABnCPn + TTA + ETA	7.99×10^{-2}	5.00×10^{-5}	9.30×10^{-3}	7.80×10^{-7}	1.0×10^{-13}	8.0×10^7	1.40	0.324
△	2013-1	[31]	BDMeABnCHx + TTA + ETA	6.75×10^{-2}	5.00×10^{-5}	1.01×10^{-2}	7.80×10^{-7}	1.0×10^{-13}	8.0×10^7	1.40	0.200
◇	2014-1	[41]	Irg819 + PETA	4.70×10^0	3.72×10^{-2}	5.00×10^{-2}	8.10×10^{-7}	1.0×10^{-13}	8.0×10^7	1.40	1.397
◇	2014-1	[41]	Irg819 + DPEPA	8.13×10^0	3.68×10^{-2}	3.78×10^{-2}	8.10×10^{-7}	1.0×10^{-13}	8.0×10^7	1.40	0.799
◇	2014-1	[41]	Irg819 + TMPTA	1.49×10^0	3.68×10^{-2}	8.84×10^{-2}	8.10×10^{-7}	1.0×10^{-13}	8.0×10^7	1.40	1.406
□	2014-1	[41]	DETC + PETA	3.09×10^1	3.72×10^{-2}	1.95×10^{-2}	8.10×10^{-7}	1.0×10^{-13}	8.0×10^7	1.40	0.286
▲	2014-1	[41]	ITX + PETA	6.27×10^0	3.68×10^{-2}	4.31×10^{-2}	8.10×10^{-7}	1.0×10^{-13}	8.0×10^7	1.40	0.845
◇	2016-1	[53]	Irg369 + DTMPA	4.52×10^{-1}	4.00×10^{-3}	5.00×10^{-2}	7.80×10^{-7}	1.0×10^{-13}	8.0×10^7	1.40	1.000
◆	2016-1	[53]	Irg369 + DTMPA + PETMP	1.57×10^0	5.00×10^{-3}	3.00×10^{-2}	7.80×10^{-7}	1.0×10^{-13}	8.0×10^7	1.40	1.000
★	2017-1	[15]	Irg369 + SZ2080	2.47×10^2	5.00×10^{-4}	6.00×10^{-5}	5.15×10^{-7}	3.0×10^{-13}	2.0×10^5	1.40	1.000
★	2017-1	[15]	Pure SZ2080	1.39×10^2	5.00×10^{-4}	8.00×10^{-5}	5.15×10^{-7}	3.0×10^{-13}	2.0×10^5	1.40	0.000
□	2019-1	[43]	DETC + PETA	2.29×10^2	1.82×10^{-1}	1.84×10^{-2}	8.00×10^{-7}	1.4×10^{-13}	8.0×10^7	1.40	0.250
□	2019-1	[43]	DETC + TMPETA	2.31×10^1	1.82×10^{-1}	5.80×10^{-2}	8.00×10^{-7}	1.4×10^{-13}	8.0×10^7	1.40	0.250
□	2019-1	[43]	DETC + BPFDA	1.35×10^2	1.82×10^{-1}	2.40×10^{-2}	8.00×10^{-7}	1.4×10^{-13}	8.0×10^7	1.40	0.250
□	2019-1	[43]	DETC + THICTA	1.60×10^2	7.28×10^{-3}	4.40×10^{-3}	8.00×10^{-7}	1.4×10^{-13}	8.0×10^7	1.40	0.250
◇	2019-1	[43]	Irg369 + PETA	5.61×10^1	1.82×10^{-1}	3.72×10^{-2}	8.00×10^{-7}	1.4×10^{-13}	8.0×10^7	1.40	2.000
◇	2019-1	[43]	Irg819 + PETA	3.04×10^1	1.82×10^{-1}	5.05×10^{-2}	8.00×10^{-7}	1.4×10^{-13}	8.0×10^7	1.40	2.000
○	2019-1	[43]	Pure PETA	6.18×10^0	1.82×10^{-1}	1.12×10^{-1}	8.00×10^{-7}	1.4×10^{-13}	8.0×10^7	1.40	0.000

Table 2. Continuation of Table 1.

Sym.	Label	Ref.	Photoresist	FOM	ν [m s ⁻¹]	P_{th} [W]	λ_0 [m]	t_p [s]	R_p [Hz]	NA	n_{pl} [wt%]
◀	2019-2	[32]	BMOA-IT + TTA + ETA	2.03×10^1	3.16×10^{-1}	9.00×10^{-2}	7.98×10^{-7}	7.2×10^{-14}	7.3×10^7	0.80	0.345
◀	2019-2	[32]	BtBuA-IT + TTA + ETA	2.57×10^1	3.16×10^{-1}	8.00×10^{-2}	7.98×10^{-7}	7.2×10^{-14}	7.3×10^7	0.80	0.398
◀	2019-2	[32]	BMA-IT + TTA + ETA	4.57×10^1	3.16×10^{-1}	6.00×10^{-2}	7.98×10^{-7}	7.2×10^{-14}	7.3×10^7	0.80	0.313
◀	2019-2	[32]	BTMSA-IT + TTA + ETA	4.57×10^0	3.16×10^{-2}	6.00×10^{-2}	7.98×10^{-7}	7.2×10^{-14}	7.3×10^7	0.80	0.430
◀	2019-2	[32]	BHA-IT + TTA + ETA	3.36×10^1	3.16×10^{-1}	7.00×10^{-2}	7.98×10^{-7}	7.2×10^{-14}	7.3×10^7	0.80	0.285
◀	2019-2	[32]	BFA-IT + TTA + ETA	3.36×10^1	3.16×10^{-1}	7.00×10^{-2}	7.98×10^{-7}	7.2×10^{-14}	7.3×10^7	0.80	0.321
◀	2019-2	[32]	BCNA-IT + TTA + ETA	3.36×10^0	3.16×10^{-2}	7.00×10^{-2}	7.98×10^{-7}	7.2×10^{-14}	7.3×10^7	0.80	0.335
◀	2019-2	[32]	BSO ₂ MA-IT + TTA + ETA	6.58×10^0	3.16×10^{-2}	5.00×10^{-2}	7.98×10^{-7}	7.2×10^{-14}	7.3×10^7	0.80	0.442
▽	2019-2	[32]	BDBAn3FL + TTA + ETA	6.43×10^0	1.00×10^{-1}	9.00×10^{-2}	7.98×10^{-7}	7.2×10^{-14}	7.3×10^7	0.80	0.317
▲	2019-3	[33]	BDAPhTX + PETA	2.09×10^{-1}	1.00×10^{-4}	5.50×10^{-3}	8.00×10^{-7}	2.5×10^{-14}	8.0×10^7	1.49	0.250
▲	2019-3	[33]	DANTX + PETA	2.56×10^{-1}	1.00×10^{-4}	4.97×10^{-3}	8.00×10^{-7}	2.5×10^{-14}	8.0×10^7	1.49	0.500
▲	2019-3	[33]	ITX + PETA	5.95×10^{-2}	1.00×10^{-4}	1.03×10^{-2}	8.00×10^{-7}	2.5×10^{-14}	8.0×10^7	1.49	1.500
◁	2019-4	[34]	36CbzDBOx + TMPTA + TMP3EOTA	1.12×10^0	7.50×10^{-4}	1.40×10^{-2}	8.00×10^{-7}	1.0×10^{-13}	8.0×10^7	1.42	0.100
◁	2019-4	[34]	36CbzDAOx + TMPTA + TMP3EOTA	1.52×10^0	7.50×10^{-4}	1.20×10^{-2}	8.00×10^{-7}	1.0×10^{-13}	8.0×10^7	1.42	0.087
◁	2019-4	[34]	27CbzDBOx + TMPTA + TMP3EOTA	1.52×10^0	7.50×10^{-4}	1.20×10^{-2}	8.00×10^{-7}	1.0×10^{-13}	8.0×10^7	1.42	0.100
◁	2019-4	[34]	27CbzDAOx + TMPTA + TMP3EOTA	4.47×10^0	7.50×10^{-4}	7.00×10^{-3}	8.00×10^{-7}	1.0×10^{-13}	8.0×10^7	1.42	0.087
●	2019-4	[34]	TPO + TMPTA + TMP3EOTA	1.28×10^0	7.50×10^{-4}	1.31×10^{-2}	8.00×10^{-7}	1.0×10^{-13}	8.0×10^7	1.42	0.045
☆	2019-4	[34]	IP-L	1.30×10^0	7.50×10^{-4}	1.30×10^{-2}	8.00×10^{-7}	1.0×10^{-13}	8.0×10^7	1.42	?
◁	2019-5	[52]	OXE + PETA	1.37×10^3	4.00×10^{-5}	2.20×10^{-4}	7.40×10^{-7}	1.4×10^{-13}	8.0×10^7	0.65	0.101
★	2019-6	[51]	Pure SZ2080	1.41×10^2	1.00×10^{-2}	1.46×10^{-4}	5.15×10^{-7}	3.0×10^{-13}	2.0×10^5	1.40	0.000
□	—	[—]	DETC + PETA	4.74×10^1	1.24×10^{-1}	2.93×10^{-2}	8.20×10^{-7}	1.0×10^{-13}	8.0×10^7	1.40	0.500
■	—	[—]	DETC + PETA + TEA	9.00×10^1	1.24×10^{-1}	2.13×10^{-2}	8.20×10^{-7}	1.0×10^{-13}	8.0×10^7	1.40	0.500
■	—	[—]	DETC + PETA + DBAm	9.00×10^1	1.24×10^{-1}	2.13×10^{-2}	8.20×10^{-7}	1.0×10^{-13}	8.0×10^7	1.40	0.500
■	—	[—]	DETC + PETA + DPIHFP	9.00×10^1	1.24×10^{-1}	2.13×10^{-2}	8.20×10^{-7}	1.0×10^{-13}	8.0×10^7	1.40	0.500
■	—	[—]	DETC + PETA + DBA + DPIHFP	1.45×10^2	1.24×10^{-1}	1.68×10^{-2}	8.20×10^{-7}	1.0×10^{-13}	8.0×10^7	1.40	0.500
○	—	[—]	Pure PETA	1.91×10^1	6.14×10^{-2}	1.13×10^{-2}	4.05×10^{-7}	1.0×10^{-13}	8.0×10^7	1.40	0.000
○	—	[—]	Pure DPHA	2.95×10^1	6.14×10^{-2}	9.07×10^{-3}	4.05×10^{-7}	1.0×10^{-13}	8.0×10^7	1.40	0.000
○	—	[—]	Pure BPADA	5.67×10^1	6.14×10^{-2}	6.54×10^{-3}	4.05×10^{-7}	1.0×10^{-13}	8.0×10^7	1.40	0.000
○	—	[—]	Pure BPAGMA	4.23×10^1	6.14×10^{-2}	7.57×10^{-3}	4.05×10^{-7}	1.0×10^{-13}	8.0×10^7	1.40	0.000
☆	—	[—]	IP-DIP	3.33×10^1	1.24×10^{-1}	3.50×10^{-2}	8.20×10^{-7}	1.0×10^{-13}	8.0×10^7	1.40	?
☆	—	[—]	IP-L	3.33×10^1	1.24×10^{-1}	3.50×10^{-2}	8.20×10^{-7}	1.0×10^{-13}	8.0×10^7	1.40	?
☆	—	[—]	IP-S	5.92×10^{-1}	2.21×10^{-3}	3.50×10^{-2}	8.20×10^{-7}	1.0×10^{-13}	8.0×10^7	1.40	?
□	—	[—]	DETC + BPADA	5.37×10^1	1.24×10^{-1}	2.76×10^{-2}	8.20×10^{-7}	1.0×10^{-13}	8.0×10^7	1.40	0.500
□	—	[—]	DETC + DPHA	7.92×10^1	1.24×10^{-1}	2.27×10^{-2}	8.20×10^{-7}	1.0×10^{-13}	8.0×10^7	1.40	0.500
□	—	[—]	DETC + UDMA	3.33×10^0	1.24×10^{-2}	3.50×10^{-2}	8.20×10^{-7}	1.0×10^{-13}	8.0×10^7	1.40	0.500
□	—	[—]	DETC + BPAGMA	1.87×10^1	6.99×10^{-2}	3.50×10^{-2}	8.20×10^{-7}	1.0×10^{-13}	8.0×10^7	1.40	0.500
■	—	[—]	DETC + PETA + PETMP	6.26×10^1	6.99×10^{-2}	1.91×10^{-2}	8.20×10^{-7}	1.0×10^{-13}	8.0×10^7	1.40	0.500
△	—	[—]	BDMeABnCHx + PETA	1.12×10^2	1.24×10^{-1}	1.91×10^{-2}	8.20×10^{-7}	1.0×10^{-13}	8.0×10^7	1.40	0.100
△	—	[—]	BDMeABnCHx + BPADA	2.13×10^2	1.24×10^{-1}	1.38×10^{-2}	8.20×10^{-7}	1.0×10^{-13}	8.0×10^7	1.40	0.400
△	—	[—]	BDBuABnCHx (BBK) + PETA	9.05×10^2	1.24×10^{-1}	6.71×10^{-3}	8.20×10^{-7}	1.0×10^{-13}	8.0×10^7	1.40	0.700

five-photon absorption of the monomer itself set in.^[48] Hence, photoinitiators are no longer needed. However, under these conditions, the microexplosion threshold typically appears at only slightly larger laser powers than the laser polymerization threshold. Such behavior makes the operation of the 3D printer

critical with respect to laser power to within some percent and, therefore, not attractive for reliable real-world application.

At focus velocities between 10 $\mu\text{m s}^{-1}$ and 1 cm s^{-1} in Figure 4, the SZ photoresists (cf. full five-pointed star symbols) exhibit FOM > 100 for fundamental excitation wavelengths

in the green, red, and infrared spectral region. SZ2080 designates a monomer mixture, which has been used in conjunction with various photoinitiators.^[50] In Figure 4, experimental data on SZ2080-mixtures containing Irgacure 369, DABP (4,4'-bis(dimethylamino)benzophenone), DETX (2,4-diethyl-9H-thioxanten-9-one), and without any photoinitiator are shown. These data correspond to low repetition rates of either $R_p = 1$ kHz or 200 kHz (cf. Tables 1 and 2). They show a pronounced increase of the FOM for increasing focus velocity v ,^[51] whereas the FOM should be constant for ideal two-photon absorption, as discussed above for DETC in PETA and BDMe-ABnCHx in BPADA, respectively. This behavior again indicates the importance of processes higher than second order. Unfortunately, we have not found experimental data for SZ photoresists at pulse repetition rates larger than $R_p = 200$ kHz and for $v > 1$ cm s⁻¹. For $R_p = 200$ kHz and $v = 0.4$ m s⁻¹, the spacing between adjacent voxels would already be 2 μ m, leading to disconnected voxels for sub- μ m voxel diameters. Based on the observations made in ref. [47], we speculate that the effective exponent of the photoresist nonlinearity, and hence the effective photoresist sensitivity, might change when going from $R_p = 200$ kHz to order $R_p = 100$ MHz repetition rates.

The largest figure-of-merit shown in Figure 4 and Tables 1 and 2 is FOM = 1368.^[52] This result has been obtained at a fairly small focus velocity of $v = 40$ μ m s⁻¹ and with a photoresist system based on the monomer PETA. The photoinitiator (OXE) is a carbazole-based two-photon absorption molecule with a chevron-shaped structure, associated with an O-acyl- α -oxoimine function, which integrates a photocleavable N–O bond. OXE requires a five-step synthesis. The authors reported that the photolysis of OXE seems relatively insensitive with respect to oxygen.^[52] This behavior suggests that the photocleavage mainly proceeds via a singlet excited state. In many other photoresists, the oxygen concentration sensitively influences the polymerization threshold power as well as the accessible spatial resolution by suppressing the proximity effect.^[41] Furthermore, in their experiments, the authors used a fairly low numerical aperture of NA = 0.6. On this basis, the achievable spatial resolution of the OXE in PETA system is presently not clear. Furthermore, it is not clear whether the FOM = 1368 of this interesting photoresist system can experimentally be carried over to state-of-the-art focus scanning velocities, which are four orders of magnitude larger than the used $v = 40$ μ m s⁻¹.

6. New Experiments

As can be seen from Tables 1 and 2, some of the data points in Figures 3 and 4 are original for the present paper, others have been remeasured by us here for previously introduced photoresists to allow for a direct comparison within this paper. In this section, we provide details for all of the photoresists corresponding to these data in Figures 3 and 4.

Experimental setups allowing for determining the threshold laser power in two-photon based 3D printing have been described many times in the literature.^[43,53] The home-built 3D laser lithography setup used here is closely similar to the one used in ref. [47]. The most important components are a

mode-locked femtosecond laser oscillator (Mai Tai HP, Spectra-Physics) operating at $R_p = 80$ MHz repetition rate and $\lambda_0 = 820$ nm center wavelength, an acousto-optic modulator, piezoelectric translation stages to move the sample with respect to the laser focus, and a focusing microscope lens (Leica HCX PL APO 100 \times /1.4–0.7 Oil CS), which is used in oil-immersion mode.^[11] The laser pulses are focused through a BK7 glass substrate into the photoresist.^[11] The liquid photoresists are drop-cast onto the glass substrate. For a chosen exposure time t_{exp} , we expose a series of spatially separated points with different laser powers P . During the exposure time, we do not move the focus with respect to the sample. After development of the photoresist using acetone, we inspect the sample by using an optical microscope and identify the minimum power, the threshold power P_{th} , that has led to a visible polymer dot. To our experience, the determined values for P_{th} vary in detail depending on which optical microscope or which imaging mode one uses or whether one rather uses electron microscopy. However, this variation is on the level of about $\pm 10\%$, which is hardly visible within the symbol size in the double-logarithmic plots in Figures 3 and 4. All laser powers are measured at the position of the objective lens through an aperture of 5.6 mm in diameter, corresponding to the objective lens entrance pupil diameter.

As the photoresist composed of PETA as a monomer and DETC as a photoinitiator has proven to be highly sensitive (see Section 5), we have considered adding cointiators to this resist system. Onium salts and amines have been reported to increase the polymerization rate and conversion.^[54] For instance, the onium salt DPIHFP (diphenyliodonium hexafluorophosphate) gets reduced by a formal electron transfer after light absorption by the photoinitiator. DPIHFP then forms unstable diaryl iodine free radicals.^[55] Amines assist the polymerization reaction by forming a charge-transfer complex with dissolved oxygen,^[56] which converts into a hydroperoxide, consuming oxygen and generating further radical species after decomposing.^[57] Through the consumption of oxygen, this process also attenuates radical inhibition.

Since both amine and onium salt can improve the performance of the photoinitiator^[58] we have investigated the incorporation of amines, i.e., a tertiary amine TEA (triethylamine) and a secondary amine DBA (dibutylamine) as well as the onium salt DPIHFP in the photoresist system. All the formulations containing PETA, DETC, and either amine or onium salt as a cointiator show slight improvements with respect to the threshold laser power. Adding both, amine and onium salt, decreases the threshold laser power even further. DBA shows a more prominent effect than TEA. However, all sensitivity improvements are comparatively small for short exposure times (corresponding to high focus velocities). Furthermore, resist systems with said cointiators show a deviation from the third-order process previously observed for pure PETA and DETC toward a second-order process, accelerating the increase of the required threshold laser power versus the focus velocity. This behavior is disadvantageous.

Alongside DETC, the photoinitiator BDMeABnCHx^[31] shows a high FOM. However, due to low solubility in commonly used monomers such as PETA, BDMeABnCHx has not surpassed the FOM of DETC based photoresists so far. To increase the solubility of BDMeABnCHx in PETA, we have modified its

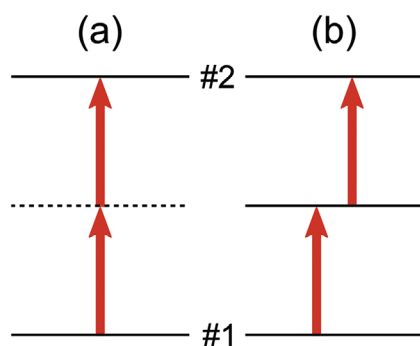


Figure 5. Schematic illustration comparing different effectively nonlinear absorption mechanisms from a lower-energy electronic state (#1) to a higher-energy electronic excited state (#2) of a molecule. Electrons in level #2 shall eventually initiate the polymerization process. a) Simultaneous two-photon absorption of laser light. The energy of the intermediate “virtual” state (dashed), halfway between levels #1 and #2, is induced by the light field itself. Its lifetime corresponds to the laser pulse duration. b) Same, but with a real intermediate state, i.e., an electronic state that exists if the light field is switched off. Here, an electron can be excited to the upper state by two sequential one-photon absorption processes. Under suitable conditions, the occupation of level #2 is proportional to the square of the laser intensity, just like for two-photon absorption in panel (a).

chemical structure: In our synthesis (see the Supporting Information), we have replaced the methyl side groups with longer alkyl chains, i.e. butyl groups, leading to the derivative BDBuABnCHx (BBK). This small variation increases the solubility in PETA by a factor of seven. Thereby, the FOM of BBK in PETA increases to $\text{FOM} = 905$ at an effective focus velocity of $v = 12.4 \text{ cm s}^{-1}$ (see Figure 4 and Table 2), which is larger by a factor of eight with respect to BDMeABnCHx in PETA. This is the largest FOM at large focus velocities reported so far.

7. Conclusion

We have reviewed more than 70 different photoresist systems that are suitable for multiphoton based 3D laser micro- and nanoprinting by scaling the raw data from the literature and the original data presented here to a dimensionless photoresist-sensitivity FOM. We find that this photoresist-sensitivity FOM varies by about six orders of magnitude from $\text{FOM} < 10^{-2}$ to $\text{FOM} > 10^3$. For six different photoresist systems, a $\text{FOM} > 10^2$ at focus velocities $v \geq 1 \text{ cm s}^{-1}$ has been demonstrated experimentally. Interestingly, many of these photoresists exhibit effective nonlinearities that are not consistent with pure two-photon absorption. A single photoresist exhibits a $\text{FOM} > 10^3$, albeit measured at a fairly small focus velocity of $v = 40 \text{ } \mu\text{m s}^{-1}$ and with unclear spatial resolution and proximity effect. Here, the behavior has been consistent with two-photon absorption. Translated back to a simple set of dimensioned quantities, a photoresist-sensitivity of $\text{FOM} = 10^2$ corresponds to a polymerization threshold laser power of $P_{\text{th}} = 100 \text{ mW}$ at a focus velocity of $v = 1 \text{ m s}^{-1}$, a fundamental laser center wavelength of $\lambda_0 = 1 \text{ } \mu\text{m}$, a pulse duration of $t_p = 100 \text{ fs}$, a pulse repetition rate of $R_p = 100 \text{ MHz}$, and at a microscope objective numerical aperture of $\text{NA} = 1$. For an array of 4×4 laser foci, the total power exiting the microscope lens would

already be as large as 1.6 W. Even for a well-engineered optical system, an overall power loss from the laser to the focusing objective lens that is smaller than a factor of two is very hard to achieve, leading to necessary femtosecond-laser powers $> 3 \text{ W}$. Therefore, further improvements in regard to photoresist sensitivity are very highly desirable, especially for high-speed multifocus multiphoton 3D laser nanoprinting^[3] or high-speed projection-based multiphoton 3D laser nanoprinting.^[12] These improvements might be accomplished by increasing the solubility of existing efficient photoinitiator molecules via chemical modifications or by the synthesis of completely novel efficient photoinitiators. For example, the recently introduced BBK and OXE photoinitiators discussed in this review go in this direction.

A possible future avenue toward sensitive nonlinear photoresists is to replace two-photon absorption by two sequential resonant one-photon absorption processes. As illustrated in Figure 5, two-photon absorption is connected to a virtual intermediate state in the middle between a lower and an upper energy level, the lifetime of which is directly determined by the femtosecond optical pulse duration. If we replace this virtual state in Figure 5a by a real electronic intermediate state with longer lifetime shown in Figure 5b, the sensitivity can potentially be increased. Suppose that the intermediate state lifetime is not too long and that the transition rate from the intermediate energy level to the upper energy level is sufficiently large. In this case, the intermediate-state population probability remains sufficiently small compared to unity at all times. Thus, the upper-state occupation and hence the exposure rate would be proportional to the square of the intensity—just like for two-photon absorption. Interestingly, an inexpensive cw laser could be used to mediate the two sequential one-photon absorption processes.

While we have emphasized the aspect of photoresist sensitivity in this review, it should be clear that many other materials aspects of photoresists are equally important for applications. Examples are the achievable spatial resolution, the size of the process window before microexplosions occur, the ease of handling, the optical refractive index, the mechanical Young's modulus, etc.

Let us finally address some yet more fundamental limits of high-speed 3D nanoprinting: Using state-of-the-art sensitive multiphoton photoresists, previous work has 3D printed a record-high number of 300 billion $= 3 \times 10^{11}$ voxels at a peak printing rate of nearly 10^7 voxels s^{-1} .^[3] Suppose that future progress yields an improved 100 nm voxel size. 3D printing a 1 cm^3 volume, equal to 10^{15} voxels, would then take 10^8 s, which is more than three years. As another example, a 1 L $= 10 \text{ cm}^3$ volume with 10 nm voxel size, corresponding to 10^{21} voxels total, would take more than 3000 years—even if the 3D printing rate was boosted up by three orders of magnitude to 10^{10} voxels s^{-1} . The number of 10^{21} voxels, equivalent to 10^{21} Bits, approaches the estimated total digital data accumulated by humankind in the year 2020, which is estimated to be around 45 billion Terabyte $= 4.5 \times 10^{22}$ Byte $> 3.6 \times 10^{23}$ Bit.^[59] This number is comparable to the Avogadro number $N_A = 6.022 \times 10^{23}$. This discussion shows that 3D printing may be boosted by more sensitive photoresists and yet higher 3D printing rates, however, it is eventually going to be limited by the enormous information

content of specimen that are large in overall volume and that contain fine features at the same time.

This dilemma asks for novel approaches. One approach that has recently been implemented in two different commercially available instruments (Nanoscribe GmbH and upnano GmbH) is to change the size and volume of the voxel dynamically over a large range during the multiphoton 3D printing process. Only where required, the minimum possible voxel size is used. Clearly, this ansatz only works for certain types of 3D architectures, e.g., for free-form surfaces. A distinct approach is to combine controllable directed self-assembly on the nanometer scale with multiphoton 3D printing on the sub-micrometer scale and above. Such demonstrations have recently emerged, too.^[60,61] All of these approaches would benefit from more sensitive multiphoton photoresists as well.

Note added in proof:

Recently, we have become aware of a submitted paper (C. Arnoux et al., DOI:10.26434/chemrxiv.12662315.v1) in which two new photoinitiators are presented, for which we derive FOM = 204 and FOM = 362, respectively.

Supporting Information

Supporting Information is available from the Wiley Online Library or from the author.

Acknowledgements

The authors thank Joachim Fischer (formerly KIT) for help regarding the numerical focus calculations following ref. [2]. They acknowledge funding by the Deutsche Forschungsgemeinschaft (DFG, German Research Foundation) under Germany's Excellence Strategy for the Excellence Cluster "3D Matter Made to Order" (2082/1– 390761711), by the Carl Zeiss Foundation, by the Helmholtz program "Science and Technology of Nanosystems," by the Karlsruhe School of Optics and Photonics (KSOP), and by the Max Planck School of Photonics (MPSP). C.B.-K. acknowledges funding from the Australian Research Council (ARC) in the context of a Laureate Fellowship enabling his photochemical research program as well as an ARC Discovery grant supporting the collaboration with M.W. This article is part of the *Advanced Optical Materials* Hall of Fame article series, which recognizes the excellent contributions of leading researchers to the field of optical materials science. Open access funding enabled and organized by Projekt DEAL.

Conflict of Interest

The authors declare no conflict of interest.

Keywords

3D additive manufacturing, 3D two-photon nanoprinting, multifocus printing, photoresist sensitivity

Received: June 2, 2020

Revised: July 23, 2020

Published online:

- [1] R. L. Truby, J. A. Lewis, *Nature* **2016**, *540*, 371.
- [2] J. Fischer, M. Wegener, *Laser Photonics Rev.* **2013**, *7*, 22.
- [3] V. Hahn, P. Kiefer, T. Frenzel, J. Qu, E. Blasco, C. Barner-Kowollik, M. Wegener, *Adv. Funct. Mater.* **2020**, *30*, 1907795.
- [4] Z.-B. Sun, X.-Z. Dong, W.-Q. Chen, S. Nakanishi, X.-M. Duan, S. Kawata, *Adv. Mater.* **2008**, *20*, 914.
- [5] F. Mayer, S. Richter, J. Westhauser, E. Blasco, C. Barner-Kowollik, M. Wegener, *Sci. Adv.* **2019**, *5*, eaau9160.
- [6] J. R. Tumbleston, D. Shirvanyants, N. Ermoshkin, R. Januszewicz, A. R. Johnson, D. Kelly, K. Chen, R. Pinschmidt, J. P. Rolland, A. Ermoshkin, E. T. Samulski, J. M. DeSimone, *Science* **2015**, *347*, 1349.
- [7] D. A. Walker, J. L. Hedrick, C. A. Mirkin, *Science* **2019**, *366*, 360.
- [8] Q. Ge, Z. Li, Z. Wang, K. Kowsari, W. Zhang, X. He, J. Zhou, N. Fang, *Int. J. Extreme Manuf.* **2020**, *2*, 2.
- [9] B. E. Kelly, I. Bhattacharya, H. Heidari, M. Shusteff, C. M. Spadaccini, H. K. Taylor, *Science* **2019**, *363*, 1075.
- [10] D. Loterie, P. Delrot, C. Moser, *Nat. Commun.* **2020**, *11*, 852.
- [11] T. Baldacchini, *Three-Dimensional Microfabrication Using Two-Photon Polymerization*, William Andrew Publishing, Oxford, UK **2016**.
- [12] S. K. Saha, D. Wang, V. H. Nguyen, Y. Chang, J. S. Oakdale, S.-C. Chen, *Science* **2019**, *366*, 105.
- [13] R. Houbertz, *Appl. Surf. Sci.* **2005**, *247*, 504.
- [14] M. Malinauskas, P. Danilevičius, S. Juodkazis, *Opt. Express* **2011**, *19*, 5602.
- [15] L. Jonušauskas, D. Gailevičius, L. Mikoliūnaitė, D. Sakalauskas, S. Šakirzanovas, S. Juodkazis, M. Malinauskas, *Materials* **2017**, *10*, 12.
- [16] M. Malinauskas, A. Žukauskas, G. Bičkauskaitė, R. Gadonas, S. Juodkazis, *Opt. Express* **2010**, *18*, 10209.
- [17] S. Maruo, O. Nakamura, S. Kawata, *Opt. Lett.* **1997**, *22*, 132.
- [18] M. Thiel, J. Fischer, G. von Freymann, M. Wegener, *Appl. Phys. Lett.* **2010**, *97*, 221102.
- [19] M. T. Do, T. T. N. Nguyen, Q. Li, H. Benisty, I. Ledoux-Rak, N. D. Lai, *Opt. Express* **2013**, *21*, 20964.
- [20] T. Bückmann, M. Thiel, M. Kadic, R. Schittny, M. Wegener, *Nat. Commun.* **2014**, *5*, 4130.
- [21] J. Kato, N. Takeyasu, Y. Adachi, H.-B. Sun, S. Kawata, *Appl. Phys. Lett.* **2005**, *86*, 044102.
- [22] S. Matsuo, S. Juodkazis, H. Misawa, *Appl. Phys. A* **2005**, *80*, 683.
- [23] B. H. Cumpston, S. P. Ananthavel, S. Barlow, D. L. Dyer, J. E. Ehrlich, L. L. Erskine, A. A. Heikal, S. M. Kuebler, I.-Y. S. Lee, D. McCord-Maughon, J. Qin, H. Röckel, M. Rumi, X.-L. Wu, S. R. Marder, J. W. Perry, *Nature* **1999**, *398*, 51.
- [24] M. Pawlicki, H. A. Collins, R. G. Denning, H. L. Anderson, *Angew. Chem., Int. Ed.* **2009**, *48*, 3244.
- [25] S. M. Kuebler, K. L. Braun, W. Zhou, J. K. Cammack, T. Yu, C. K. Ober, S. R. Marder, J. W. Perry, *J. Photochem. Photobiol., Chem.* **2003**, *158*, 163.
- [26] J. Gu, W. Yulan, W.-Q. Chen, X.-Z. Dong, X.-M. Duan, S. Kawata, *New J. Chem.* **2007**, *31*, 63.
- [27] J.-F. Xing, W.-Q. Chen, J. Gu, X.-Z. Dong, N. Takeyasu, T. Tanaka, X.-M. Duan, S. Kawata, *J. Mater. Chem.* **2007**, *17*, 1433.
- [28] J.-F. Xing, X.-Z. Dong, W.-Q. Chen, X.-M. Duan, N. Takeyasu, T. Tanaka, S. Kawata, *Appl. Phys. Lett.* **2007**, *90*, 131106.
- [29] X. Cao, F. Jin, Y.-F. Li, W.-Q. Chen, X.-M. Duan, L.-M. Yang, *New J. Chem.* **2009**, *33*, 1578.
- [30] J.-F. Xing, M.-L. Zheng, W.-Q. Chen, X.-Z. Dong, N. Takeyasu, T. Tanaka, Z.-S. Zhao, X.-M. Duan, S. Kawata, *Phys. Chem. Chem. Phys.* **2012**, *14*, 15785.
- [31] Z. Li, N. Pucher, K. Cicha, J. Torgersen, S. C. Ligon, A. Ajami, W. Husinsky, A. Rosspeintner, E. Vauthey, S. Naumov, T. Scherzer, J. Stampfl, R. Liska, *Macromolecules* **2013**, *46*, 352.
- [32] B. Holzer, M. Lunzer, A. Rosspeintner, G. Licari, M. Tromayer, S. Naumov, D. Lumpi, E. Horkel, C. Hametner, A. Ovsianikov, R. Liska, E. Vauthey, J. Fröhlich, *Mol. Syst. Des. Eng.* **2019**, *4*, 437.

- [33] T. Chi, P. Somers, D. A. Wilcox, A. J. Schuman, V. Iyer, R. Le, J. Gengler, M. Ferdinandus, C. Liebig, L. Pan, X. Xu, B. W. Boudouris, *J. Polym. Sci., Part B: Polym. Phys.* **2019**, 57, 1462.
- [34] P. Hu, W. Qiu, S. Naumov, T. Scherzer, Z. Hu, Q. Chen, W. Knolle, Z. Li, *ChemPhotoChem* **2020**, 4, 224.
- [35] W.-E. Lu, X.-Z. Dong, W.-Q. Chen, Z.-S. Zhao, X.-M. Duan, *J. Mater. Chem.* **2011**, 21, 5650.
- [36] E. Frick, C. Schweigert, B. B. Noble, H. A. Ernst, A. Lauer, Y. Liang, D. Voll, M. L. Coote, A.-N. Unterreiner, C. Barner-Kowollik, *Macromolecules* **2016**, 49, 80.
- [37] D. E. Fast, A. Lauer, J. P. Menzel, A.-M. Kelterer, G. Geschiedt, C. Barner-Kowollik, *Macromolecules* **2017**, 50, 1815.
- [38] P. Mueller, M. Thiel, M. Wegener, *Opt. Lett.* **2014**, 39, 6847.
- [39] A. Wickberg, A. Abass, H.-H. Hsiao, C. Rockstuhl, M. Wegener, *Adv. Opt. Mater.* **2019**, 7, 1801235.
- [40] A. Taguchi, A. Nakayama, R. Oketani, S. Kawata, K. Fujita, preprint arXiv:1911.03526, **2019**.
- [41] J. B. Mueller, J. Fischer, F. Mayer, M. Kadic, M. Wegener, *Adv. Mater.* **2014**, 26, 6566.
- [42] A. Pikulin, N. Biturin, *Multiphoton Lithography*, Wiley-VCH, Weinheim **2016**, pp. 65–93.
- [43] L. Yang, A. Münchinger, M. Kadic, V. Hahn, F. Mayer, E. Blasco, C. Barner-Kowollik, M. Wegener, *Adv. Opt. Mater.* **2019**, 7, 1901040.
- [44] A. S. van de Nes, L. Billy, S. F. Pereira, J. J. M. Braat, *Opt. Express* **2004**, 12, 1281.
- [45] B. E. A. Saleh, M. C. Teich, *Fundamentals of Photonics*, Wiley, New York **2007**.
- [46] V. Hahn, F. Mayer, M. Thiel, M. Wegener, *Opt. Photonics News* **2019**, 30, 28.
- [47] J. Fischer, M. Wegener, *Opt. Mater. Express* **2011**, 1, 614.
- [48] J. Fischer, J. B. Mueller, J. Kaschke, T. J. A. Wolf, A.-N. Unterreiner, M. Wegener, *Opt. Express* **2013**, 21, 26244.
- [49] B. Harke, P. Bianchini, F. Brandi, A. Diaspro, *ChemPhysChem* **2012**, 13, 1429.
- [50] A. Ovsianikov, A. Gaidukeviciute, B. N. Chichkov, M. Oubaha, B. D. MacCraith, I. Sakellari, A. Giakoumaki, D. Gray, M. Vamvakaki, M. Farsari, C. Fotakis, *Laser Chem.* **2008**, 2008, 493059.
- [51] L. Jonušauskas, D. Gailevičius, S. Rekštytė, T. Baldacchini, S. Juodkakis, M. Malinauskas, *Opt. Express* **2019**, 27, 15205.
- [52] R. Zhou, J.-P. Malval, M. Jin, A. Spangenberg, H. Pan, D. Wan, F. Morlet-Savary, S. Knopf, *Chem. Commun.* **2019**, 55, 6233.
- [53] L. Jiang, W. Xiong, Y. Zhou, Y. Liu, X. Huang, D. Li, T. Baldacchini, L. Jiang, Y. Lu, *Opt. Express* **2016**, 24, 13687.
- [54] F. A. Ogluari, C. Ely, C. L. Petzhold, F. F. Demarco, E. Piva, *J. Dent.* **2007**, 35, 583.
- [55] Y. Hua, F. Jiang, J. V. Crivello, *Chem. Mater.* **2002**, 14, 2369.
- [56] H. Tsubomura, T. Yagishita, H. Toi, *Bull. Chem. Soc. Jpn.* **1973**, 46, 3051.
- [57] R. Sato, T. Kurihara, M. Takeishi, *Polym. Int.* **1998**, 47, 159.
- [58] J.-P. Fouassier, F. Morlet-Savary, J. Lalevée, X. Allonas, C. Ley, *Materials* **2010**, 3, 5130.
- [59] D. Reinsel, J. Gantz, J. Rydning, *The Digitization of the World – From Edge to Core*, An IDC White Paper, US44413318, **2018**.
- [60] J. Greenhall, B. Raeymaekers, *Adv. Mater. Technol.* **2017**, 2, 1700122.
- [61] F. Mayer, D. Ryklin, I. Wacker, R. Curticean, M. Čalkovský, A. Niemeyer, Z. Dong, P. A. Levkin, D. Gerthsen, R. R. Schröder, M. Wegener, *Adv. Mater.* **2020**, 2002044.



Pascal Kiefer is a Ph.D. student in physics under the supervision of Prof. Martin Wegener. His research interests lie in the development of sensitive photoresist as well as parallelization methods for 3D microprinting. He is a physicist by training and obtained his Master's degree in 2019 from Karlsruhe Institute of Technology (KIT) in Karlsruhe, Germany. From 2012 to 2018, he worked at Fraunhofer Institute of Optronics, System Technologies and Image Exploitation (IOSB) in Ettlingen, Germany. In 2019, he did a research internship at the Institute for Integrated Cell-Material Sciences (iCeMS) in Kyoto, Japan.



Vincent Hahn studied physics at the Karlsruhe Institute of Technology (KIT) in Germany and obtained his master's degree in 2016. In 2014, he did a research visit at the University of Illinois at Urbana-Champaign (USA). Before starting his Ph.D. in 2016, he worked for Trumpf Photonics Inc. in Cranbury, NJ (USA). During his Ph.D. within Martin Wegener's group at KIT, his research focus lies on parallelization methods for 3D microprinting.



Martin Wegener completed his diploma and Ph.D. in physics at Johann Wolfgang Goethe-Universität Frankfurt (Germany) in 1986 and 1987, respectively. He then spent two years as a postdoc at AT&T Bell Laboratories in Holmdel (USA). From 1990 to 1995, he was a professor at Universität Dortmund (Germany). Since 1995, he has been a professor at the Institute of Applied Physics of Karlsruhe Institute of Technology (KIT). Since 2016, he has additionally been a director at Institute of Nanotechnology. Since 2018, he has been a spokesperson of the Cluster of Excellence 3D Matter Made to Order.